Published by JScE as Proceedings of 4th International Conference on Role of Energy on Sustainable Social Development (RESSD-2025), 29-30 May, 2025, Kathmandu, Nepal

ANALYSIS OF MULTIPLE BROKEN ROTOR BAR FAULT IN INDUCTION MOTOR

Shreeshuva Maharjan[1*], Bishal Silwal[2], Muhammad Usman Sardar[3], Hadi Ashraf Raja[3], Toomas Vaimann[3]

[1] Department of Electrical and Electronics Engineering, Kathmandu University
[2] Department of Electrical Engineering, Pulchowk Campus, IOE, Tribhuvan University
[3] Department of Electrical Power Engineering and Mechatronics, Tallinn University of Technology

Abstract

Induction motors are widely used in industrial applications due to their durability, simplicity, and low cost. They are, however, susceptible to a variety of faults during operation, one of the most critical of which are broken rotor bar (BRB) faults, which have the potential to cause severe performance degradation and unexpected downtime. This study describes an effective diagnostic approach for detecting BRB faults using Motor Current Signature Analysis (MCSA). The Fast Fourier Transform (FFT) was used to extract the fault-related features and the Hann's windowing function was used to minimize the spectral leakage caused by the non-stationary nature of the stator current signal. The experimental stator current data was taken for healthy and faulty motor (BRB) conditions at different load conditions. The frequency domain analysis showed distinct sideband components whose characteristics varied according to fault severity and loading. Additionally, motors under full load revealed more defined spectral features, making fault detection more reliable. The findings demonstrate that this FFT-based approach, enhanced by appropriate windowing, provides an effective and non-invasive solution for early detection of rotor faults in an induction motor.

Keywords: Induction motor, Broken rotor bar, FFT, Condition monitoring, MCSA

1. Introduction

Induction Motors (IMs) are the workhorses and critical machines of any industry due to their robustness, simplicity, high power-to-weight ratio, and efficiency (Gangsar and Tiwari, 2020; Juez-Gil et al., 2020). Pumps, compressors, cranes, electric vehicles, and fans are some of the applications where the IM is extensively used. IM operates in extreme industrial and environmental conditions and witnesses different types of stress during operation, including mechanical, thermal, electrical, and environmental stresses. This is due to variation in the loading condition, frequent starting, inadequate lubrication, manufacturing defect, dusty environment, and natural aging (Kudelina et al., 2020; Rosero et al., 2006). These stresses could lead to component failure, and any component failure could lead to the failure of IM. These faults, when persists for a longer duration, could bring out huge losses to the industries and may also risk human lives. Therefore, early fault detection and diagnosis of such faults, using an appropriate technique, is necessary in order to minimize the downtime and optimize the overall efficiency (Kumar and Hati, 2021).

The principal components of IM are the stator, rotor, and bearings. One of the most common faults in IM is a rotor fault. The several rotor faults include Broken Rotor Bar (BRB) fault, rotor misalignment, and air-gap eccentricity. According to the survey conducted by IEEE and EPRI, the fault contribution by the rotor is 8%, and 9% respectively (Albrecht et al., 1986; Society and Committee, 1980). These faults can be mitigated early by detecting the deviations from normal operating conditions. The most widely used condition monitoring technique to identify BRB fault is motor current signature analysis (MCSA) (Kudelina et al., 2021). MCSA is an effective, non-intrusive technique that detects electrical signals from

*Corresponding author: Shreeshuva Maharjan
Department of Electrical and Electronics Engineering, KU
Email: shreeshuva1323@student.ku.edu.np
https://doi.org/10.3126/jsce.v12i2.91412

the motor containing current components, which are by-products of the unique rotating flux caused by BRB faults. Therefore, MCSA effectively detects BRB related sideband components, which make it highly sensitive and reliable for fault diagnosis of BRB, as compared to other techniques, such as vibration analysis, thermal imaging, etc. The main parts associated with the condition monitoring system are data acquisition, signal processing, feature extraction, and, hence, the diagnosis of faults using their characteristics component. The methodology adopted is shown in Figure 1. Initially, the time-domain data is acquired from the data acquisition system, which is then transformed into the frequency-domain to extract the fault-related features by applying suitable signal processing techniques. The most widely used signal processing technique in fault detection is Fast Fourier Transform (FFT), which provides the current frequency spectrum of the recorded time-domain signal. According to the obtained frequency and amplitudes, the condition of the motor is identified.

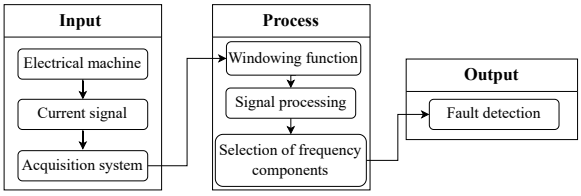

Figure 1. Block diagram of methodology

The paper is organized as follows: section 2 outlines the causes, effects, and characteristics component of the BRB fault. The section 3 describes the FFT. The experimental setup used for the analysis is discussed in section 4. The results and discussion are presented in section 5, and the paper is concluded in section 6.

2. Broken Rotor Bar Fault

BRB is one of the most common electrical faults in a squirrel-cage induction motor. The fault occurs when one or more rotor bars break or crack due to mechanical stress, thermal expansion, or manufacturing defects (Gangsar and Tiwari, 2020; Nandi et al., 2005). Mechanical stress, such as continuous mechanical loads, vibrations, and misalignment, can induce fatigue failure in rotor bars. Also, frequent start-stop cycles and high operating temperatures cause material expansion and contraction, which leads to cracks in bars (Gangsar and Tiwari, 2020). The manufacturing defect, such as poor casting, air pockets, or material inconsistencies during production, can also create weak points in the rotor bars. So, these issues, if left unaddressed, can worsen the fault, and fragments of the broken rotor bar may strike the stator's end winding, further causing severe damage (Sharma et al., 2017). Also, the current consumed by the motor will increase by 50% of the rated current, and the efficiency will be reduced, which in turn generates the excessive heat in the adjacent rotor bars (Gundewar and Kane, 2021). The Figure 2 shows the distribution of current density across the healthy motor, the 1BRB fault motor, and two adjacent BRB faults. It can be seen that the current density increases near broken bars, which, over time, can lead to the propagation of the fault. When any rotor bar is broken, it generates so-called

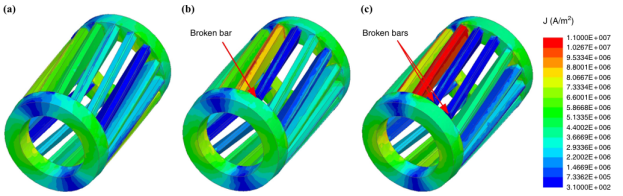

Figure 2. Distribution of current density in squirrel cage induction motor: (a) Healthy cage, (b) Cage of 1BRB, (c) Cage of continuous 2BRB (Xie et al., 2016).

sideband components in the frequency spectrum of the stator current (Benbouzid, 2002). These sidebands appear on either side of the fundamental frequency and are known as lower and upper sidebands. The lower sideband lies on the left side of the fundamental frequency, which is caused by electrical and magnetic asymmetries in the induction motor rotor cage (Bellini et al., 2001). The upper sideband is situated on the right side of the fundamental frequency, and is due to consequent speed oscillations caused by the resulting torque pulsations (Filippetti et al., 1998). A symmetrical three-phase stator winding produces a forward rotating magnetic field at synchronous speed, whereas any asymmetry in the rotor leads to a backward rotating component. In an induction motor, rotor currents create a magnetic field at slip frequency, and rotor asymmetries, such as broken bars, introduce sideband frequencies in the stator current, as given by (Gundewar and Kane, 2021; Kanović et al., 2013; Nandi et al., 2005),

$$f_b = (1 \pm 2ks) f_s \tag{1}$$

where, f_b = frequency of broken rotor bar,
s = per unit slip of motor,
f_s = supply frequency, and
k = integer (1,2,3,...).
This results in sidebands at $\pm 2sf_s$ around the fundamental frequency component. The frequency given by Equation (1) is highly slip-dependent. At a low value of slip, the sideband components are closer to the central frequency, which can cause difficulty in fault detection. Therefore, stator current signals must be acquired when the motor is operating close to full load, so that sideband components can be clearly distinguished from the

fundamental frequency.
Also, the amplitude of the sideband component provides valuable information about the rotor's condition. In a normally operating motor, the amplitude of the sidebands remains low, whereas an increase in these components often signals an issue such as cracked or broken bars. A higher sideband amplitude means a smaller difference from the fundamental component, which indicates a greater likelihood of rotor failure. The motor is said to be in good condition if the difference in amplitude between the fundamental and Left Sideband Component (LSB) is greater than 50 dB (Sharma et al., 2017). Also, if the difference lies between 40 and 50 dB, it is likely that a single broken bar is present, whereas a difference of less than 40 dB typically indicates a more severe fault, possibly involving multiple broken bars (Wahba, 2021).

3. Fast Fourier Transform

FFT is a conventional signal processing technique to convert a time-domain signal into its frequency-domain representation. This transformation helps in identifying periodic components, harmonics, and fault-related frequency signatures from the motor's signal. The large time-domain data is repeatedly divided into smaller subsets, and each subset undergoes processing before the results are systematically combined to compute the final frequency-domain representation (Akbar et al., 2023). The FFT is defined as (Kudelina et al., 2020),

$$f(t) = \sum_{n=-\infty}^{\infty} C_n e^{in\omega t} \approx \sum_{n=1}^{N} C_n e^{in\omega t}; \omega = 2\pi \frac{f}{f_s}; \quad (2)$$

$$C_n = \frac{1}{2\pi} \int_{-\infty}^{\infty} f(x) e^{-inx} dx, n = 0, \pm 1, \pm 2, ... \quad (3)$$

where, $f(x)$ = original time signal,
C_n = complex Fourier, and
f_s = sampling frequency.
Despite the efficiency of FFT, it assumes the signal to be stationary over the analysis window, meaning its frequency content does not change with time (Benbouzid, 2002). However, in real cases, the signals are often non-stationary, and the finite-length nature of sampled data introduces abrupt edges, leading to spectral leakage in the frequency-domain (Benbouzid, 2002). To mitigate this effect, windowing functions are applied to the signal before performing the FFT.

4. Experimental Setup

The stator current data corresponding to both healthy and faulty operating conditions used in this study were obtained from the experimental setup at Tallinn University of Technology, Estonia. Figure 3 shows the experimental setup used for the data acquisition.

The setup consisted of two identical induction motors,

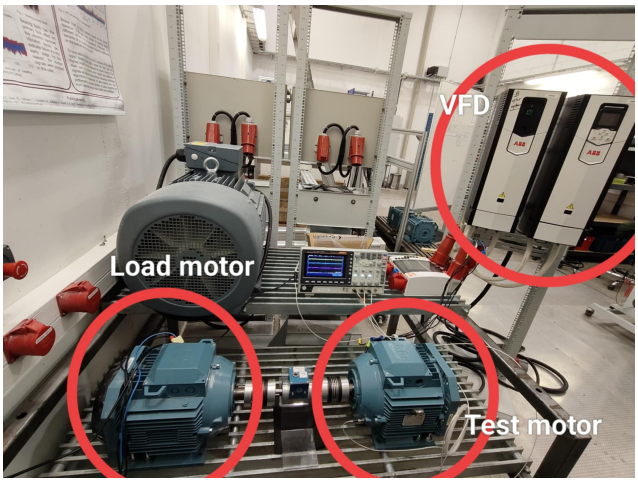

Figure 3. Experimental test rig.

which are mechanically coupled by a common shaft. One motor, operating in a completely healthy state, was used to apply the mechanical load, while the second one served as the test motor, where the test was conducted by introducing faults, specifically up to 3 BRB's, to simulate the fault conditions. The Variable Frequency Drive (VFD) was used to control both motors. The stator current data was acquired at a sampling rate of 20 kHz. The test was performed at the rated speed. The rotor with 1BRB, 0BRB (Healthy), and 2BRB (from left to right in sequence) is shown in Figure 4. The parameters of the testing motor are shown in Table 1.

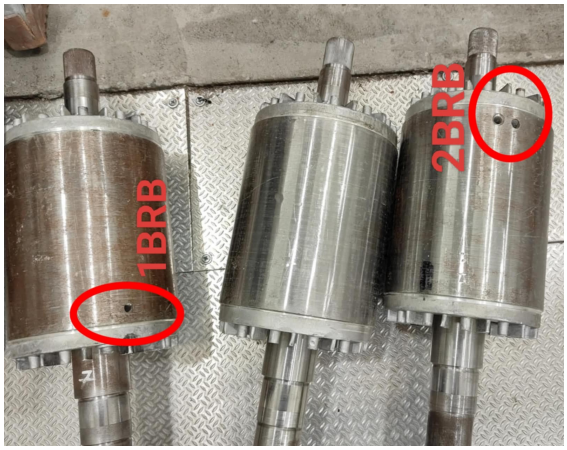

Figure 4. Single BRB, Healthy rotor bar, and double BRB.

5. Results and Discussion

The study addressed the real-world case of fault detection of an induction motor. In this study, various conditions of rotor bars in induction machines were

Table 1. Parameters of testing and loading motor

Parameter	**Value**		
Voltage, V	Y 690	Δ 400	Δ 460
Frequency, Hz	50	50	60
Speed, r/min	1460	1460	1760
Power, kW	7.5	7.5	7.5
Current, A	8.8	15.3	12.9
Power factor	0.79	0.79	0.81

examined. To facilitate the interpretation of results, the fault conditions are labeled based on the number of broken rotor bars (BRBs) introduced in the test motor, as follows:

- 0BRB: Represents the healthy condition with no broken rotor bar.
- 1BRB: Indicates the presence of one broken rotor bar in the test motor.
- 2BRB: Corresponds to two broken rotor bars.
- 3BRB: Represents the most severe case with three broken rotor bars.

Figure 5 represents the time-domain stator current signals for the motor operating under healthy (0BRB) and faulty (1BRB–3BRB) conditions at 100% rated load, captured over a time interval of 0 to 0.2 seconds. However, these

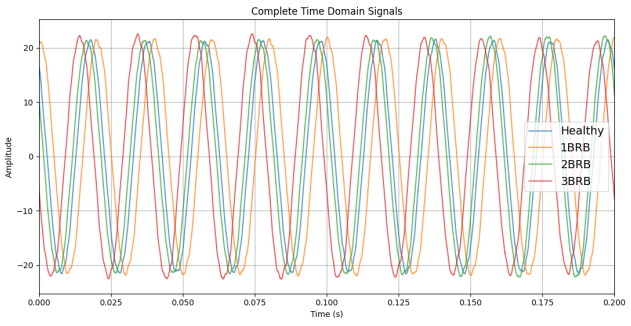

Figure 5. Stator current signals of healthy and faulty motor for 100% of rated load within time-frame from 0-0.2 seconds.

time-domain signals do not contribute significantly to the fault diagnosis. So, it is transformed into frequency-domain using FFT, so that more fault-related characteristics can be extracted. The frequency current spectra of the measured stator current signal at various load levels, along with different motor conditions is shown from Figure 6, Figure 7, Figure 8, Figure 9 and Figure 10.

In Figure 6, the plot exhibits a dominant peak at the fundamental supply frequency (50 Hz), with minimal presence of additional frequency components. However, in the case of 25% of rated load, in Figure 7, the plot comprises additional sideband components symmetrically located around the fundamental frequency. Also, the amplitudes of those sideband components are seen to be more pronounced as the number of broken rotor bars increases, thus indicating the presence of fault-induced harmonics. These sideband components, often referred to as fault harmonics, arise due to rotor asymmetry and periodic fluctuations in air-gap flux caused by the broken rotor bars. As the motor load increases, the amplitudes of the characteristic sideband components around the fundamental frequency also tend to increase. Additionally, with higher loading conditions, these symmetrical sideband components appear at greater frequency separations from the fundamental frequency. This behavior arises from the fact that the frequency components induced by broken rotor bars are strongly dependent on the motor's slip, which increases with load. As previously discussed on Equation (1), the frequency spectrum of the faulty motor clearly demonstrates a sideband at $\pm 2sf_s$ around the fundamental frequency, which is a characteristic signature of BRB faults.

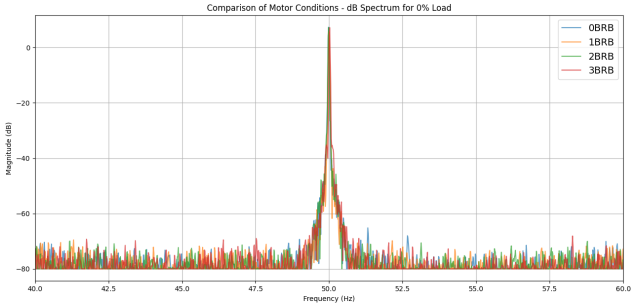

Figure 6. Frequency current spectra of various machine state at no-load.

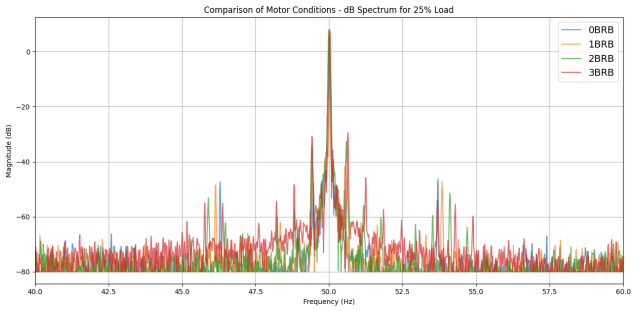

Figure 7. Frequency current spectra of various machine state at 25% of rated load.

For the case of 100% of rated load, as shown in Figure 10, the magnitude of fundamental component was found to be,
For 0BRB (healthy motor): 13.40 dB
For 3BRB (faulty motor): 14.50 dB
Also, the magnitude of LSB component for both 0BRB and

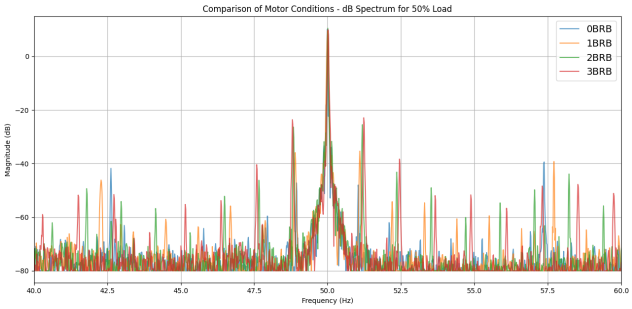

Figure 8. Frequency current spectra of various machine state at 50% of rated load.

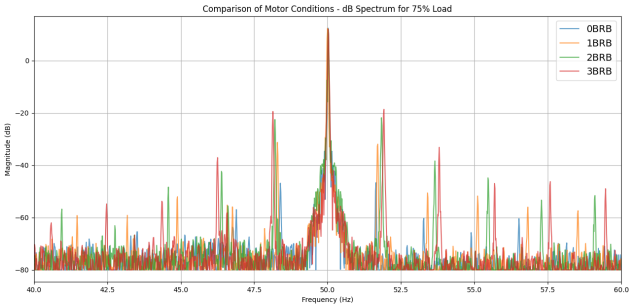

Figure 9. Frequency current spectra of various machine state at 75% of rated load.

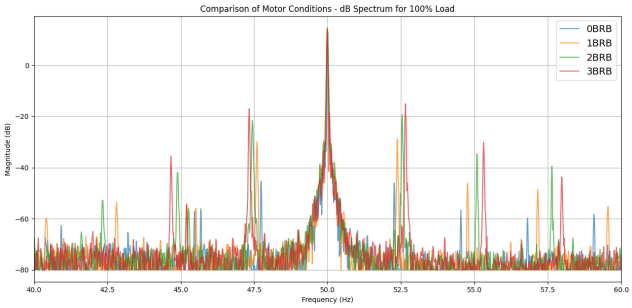

Figure 10. Frequency current spectra of various machine state at 100% of rated load.

3BRB was found to be,
For 0BRB (healthy motor): -45.30 dB
For 3BRB (faulty motor): -16.97 dB
The difference in amplitude of fundamental component and LSB of 0BRB and 3BRB is given as,
Difference between fundamental component and LSB_1 for 0BRB = 13.40 - (- 45.30) = 58.70 dB
This difference of more than 50 dB indicates that the condition of the motor is good, and no maintenance is required.
Whereas, difference between fundamental component and LSB_1 for 3BRB = 14.50 - (- 16.97) = 31.47 dB
But for this case, the difference of less than 40 dB confirms the presence of multiple broken rotor bars, indicating a critical fault condition. Immediate replacement of the damaged rotor bars is necessary to prevent further degradation of other components within the induction motor, ensuring its reliable operation and longevity.

6. Conclusion

This study focused on the detection of broken rotor bar faults in an induction motor using FFT. In order to mitigate the spectral leakage for the non-stationary stator current signal, the Hann's windowing function was used. The analysis revealed that the amplitudes and frequency spacing of the sideband components increase with both the severity of the rotor fault and the motor loading condition. In particular, at full-load condition, the amplitude difference between the fundamental component and the left sideband reduced from 58.70 dB for the healthy motor to 31.47 dB for the severely fault case, confirming the presence of multiple broken rotor bars. Notably, the progressive rise in the amplitude of these sideband components should be carefully monitored, as it may serve as an early warning indicator. This helps to allow corrective measures to be taken before the fault escalates into a more severe or cascading failure within the motor.

Acknowledgments

This work is supported by the Capacity Enhancement in Electrical Equipment Condition Monitoring and Fault Diagnostics (CEEECoM) project (Grant ID: 101082996).

References

Akbar, S., Vaimann, T., Asad, B., Kallaste, A., Sardar, M. U., & Kudelina, K. (2023). State-of-the-art techniques for fault diagnosis in electrical machines: Advancements and future directions. *Energies*, *16*(17), 6345.

Albrecht, P., Appiarius, J., McCoy, R., Owen, E., & Sharma, D. (1986). Assessment of the reliability of motors in utility applications-updated. *IEEE Transactions on Energy conversion*, (1), 39–46.

Bellini, A., Filippetti, F., Franceschini, G., Tassoni, C., & Kliman, G. B. (2001). Quantitative evaluation of induction motor broken bars by means of electrical signature analysis. *IEEE Transactions on industry applications*, *37*(5), 1248–1255.

Benbouzid, M. E. H. (2002). A review of induction motors signature analysis as a medium for faults detection. *IEEE transactions on industrial electronics*, *47*(5), 984–993.

Filippetti, F., Franceschini, G., Tassoni, C., & Vas, P. (1998). Ai techniques in induction machines diagnosis including the speed ripple effect. *IEEE Transactions on Industry Applications*, *34*(1), 98–108.

Gangsar, P., & Tiwari, R. (2020). Signal based condition monitoring techniques for fault detection and diagnosis of induction motors: A state-of-the-art review. *Mechanical systems and signal processing*, *144*, 106908.

Gundewar, S. K., & Kane, P. V. (2021). Condition monitoring and fault diagnosis of induction motor. *Journal of Vibration Engineering & Technologies*, *9*, 643–674.

Juez-Gil, M., Saucedo-Dorantes, J. J., Arnaiz-González, Á., López-Nozal, C., García-Osorio, C., & Lowe, D. (2020). Early and extremely early multi-label fault diagnosis in induction motors. *ISA transactions*, *106*, 367–381.

Kanović, Ž., Matić, D., Jeličić, Z., Rapaić, M., Jakovljević, B., & Kapetina, M. (2013). Induction motor broken rotor bar detection using vibration analysis—a case study. *2013 9th IEEE international symposium on diagnostics for electric machines, power electronics and drives (SDEMPED)*, 64–68.

Kudelina, K., Asad, B., Vaimann, T., Belahcen, A., Rassõlkin, A., Kallaste, A., & Lukichev, D. V. (2020). Bearing fault analysis of bldc motor for electric scooter application. *Designs*, *4*(4), 42.

Kudelina, K., Vaimann, T., Asad, B., Rassõlkin, A., Kallaste, A., & Demidova, G. (2021). Trends and challenges in intelligent condition monitoring of electrical machines using machine learning. *Applied Sciences*, *11*(6), 2761.

Kumar, P., & Hati, A. S. (2021). Review on machine learning algorithm based fault detection in induction motors. *Archives of Computational Methods in Engineering*, *28*(3), 1929–1940.

Nandi, S., Toliyat, H. A., & Li, X. (2005). Condition monitoring and fault diagnosis of electrical motors—a review. *IEEE transactions on energy conversion*, *20*(4), 719–729.

Rosero, J. A., Cusido, J., Garcia, A., Ortega, J., & Romeral, L. (2006). Broken bearings and eccentricity fault detection for a permanent magnet synchronous motor. *IECON 2006-32nd Annual Conference on IEEE Industrial Electronics*, 964–969.

Sharma, A., Mathew, L., & Chatterji, S. (2017). Analysis of broken rotor bar fault diagnosis for induction motor. *2017 International Conference on Innovations in Control, Communication and Information Systems (ICICCI)*, 1–5.

Society, I. I. A., & Committee, I. I. A. S. P. S. T. (1980). *Ieee recommended practice for the design of reliable industrial and commercial power systems*. Institute of Electrical & Electronics Engineers (IEEE).

Wahba, M. D. H. (2021). Using motor current signatute analysis to detect the number of broken rotor bars in induction motors.

Xie, Y., Wang, Z., Shan, X., & Li, Y. (2016). Investigation of rotor thermal stress in squirrel cage induction motor with broken bar faults. *COMPEL-The international journal for computation and mathematics in electrical and electronic engineering*, *35*(5), 1865–1886.